Wavelength-modulated differential photothermal radiometry: Theory and experimental applications to glucose detection in water

Andreas Mandelis and Xinxin Guo*

Center for Advanced Diffusion-Wave Technologies, Department of Mechanical and Industrial Engineering, University of Toronto, Toronto, Ontario, Canada M5S 3G8

(Received 30 March 2011; revised manuscript received 13 August 2011; published 14 October 2011)

A differential photothermal radiometry method, wavelength-modulated differential photothermal radiometry (WM-DPTR), has been developed theoretically and experimentally for noninvasive, noncontact biological analyte detection, such as blood glucose monitoring. WM-DPTR features analyte specificity and sensitivity by combining laser excitation by two out-of-phase modulated beams at wavelengths near the peak and the base line of a prominent and isolated mid-IR analyte absorption band (here the carbon-oxygen-carbon bond in the pyran ring of the glucose molecule). A theoretical photothermal model of WM-DPTR signal generation and detection has been developed. Simulation results on water-glucose phantoms with the human blood range (0–300 mg/dl) glucose concentration demonstrated high sensitivity and resolution to meet wide clinical detection requirements. The model has also been validated by experimental data of the glucose-water system obtained using WM-DPTR.

DOI: 10.1103/PhysRevE.84.041917 PACS number(s): 87.85.fk, 87.19.xv, 87.85.Ox, 87.80.Dj

I. INTRODUCTION

Diabetes has become one of the leading causes of death and disability in the world [1]. Patients can be at risk of heart and kidney failure, blindness, and amputations [2]. For proper diabetes management, frequent monitoring of blood glucose is required [3]. The current standard technique for self-monitoring of blood glucose requires a skin puncture to draw a small blood sample. However, the discomfort and pain of the procedure lead to poor compliance. Quick, reliable, and pain-free testing are three highly desirable characteristics for patients.

Over the past two decades the pursuit of noninvasive methods for glucose monitoring has resulted in the development of a number of optical technologies [4,5]. The near-infrared (NIR) spectral range has been well explored because of the relatively low water absorption [4,6]. However, the NIR glucose absorption bands are weak (overtone and combination bands) and are overlapped with other blood constituents. Separation often requires sophisticated processing algorithms. In comparison, the mid-infrared (MIR) region is extremely useful for glucose identification. Of particular significance is the prominent absorption peak in the 8.5–10.5-μm band which is due to the carbon-oxygen-carbon bond in the pyran ring of glucose. This feature is peaked at $\sim$9.7 μm, and is isolated from other interfering peaks in human blood [7–12]. A major difficulty of purely optical detection methods using the MIR is the intrinsic high background absorption coefficient of water which tends to fully dominate the relatively low absorption of normal glucose concentration in human blood.

Recently, a new approach to the noninvasive detection of glucose was developed. This new methodology, wavelength-modulated differential photothermal radiometry (WM-DPTR) [13], involves the measurement of glucose in a sample by means of differential detection of thermal infrared (thermophotonic) emissions produced by two incident optical beams. The differential detection is achieved by square-wave modulating the intensity of the two beams 180° out of phase, and selecting the wavelengths of the two beams to be on and off the glucose absorption peak near 9.7 μm. The simulation results from aqueous glucose mixtures 0–300 mg/dl (0–17 mmol/l) demonstrate distinct advantages of WM-DPTR over noninvasive optical methods. While developed for glucose measurements, this technique could be easily adapted to the measurements of other analytes in biomedical samples.

II. WM-DPTR THEORY

The theoretical analysis of the WM-DPTR signal comprises differential photothermal radiometric signal generation following sequential optical absorption of two out-of-phase square-wave modulated laser beams by a semi-infinite one-dimensional medium. The sensitive analyte detection is based on the selective absorption of the analyte at two excitation wavelengths (peak and base line). The differential signal arises because the absorption maximum (one laser beam) generates a photothermal-wave centroid for the IR emission closer to the surface than the absorption minimum (the other laser beam). In addition, changes in the thermophysical properties of the water-analyte mixture compared to those of pure water act as a differential signal amplifier in WM-DPTR.

A. General PTR signal formalism for transient temperature rise

When light is absorbed by a *semi-infinite one-dimensional* medium, for example, water or a water-glucose mixture, the transient temperature field of the medium can be expressed as

$$T_m(z,t) = T_0 + \Delta T_m(z,t), \tag{1}$$

where T_0 is the thermal equilibrium temperature and $\Delta T_m(z,t)$ is the temperature increase in the medium. The resulting IR radiation intensity is described by the Planck distribution function:

$$W_p(z,\lambda,T_m) = W_p(\lambda,T_0) + \Delta W_p[\lambda,T_m(z,t)], \tag{2}$$

*guox@mie.utoronto.ca

where

$$W_p(\lambda,T_0)=\frac{2\pi hc^2}{\lambda^5[\exp(hc/\lambda k_B T_0)-1]}$$

is the Planck distribution function (blackbody spectral radiant emittance at IR wavelength λ) at thermal equilibrium, and

$$\Delta W_p[\lambda,T_m(z,t)]=\frac{W_p(\lambda,T_0)(hc/\lambda k_B T_0)}{[\exp(hc/\lambda k_B T_0)-1]}\left[\frac{\Delta T_m(z,t)}{T_0}\right]$$

is the IR radiation increase due to the temperature increase. Here, h is Planck's constant, c is the speed of light in vacuum, and k_B is the Boltzmann constant. The IR radiation emitted and intercepted by an IR detector is

$$\begin{aligned}Q(t;\lambda_1,\lambda_2)&=[1-R(\lambda_{\rm exc})]\int_0^\infty\int_{\lambda_1}^{\lambda_2}\mu_{\rm IR}(\lambda)e^{-\mu_{\rm IR}(\lambda)z}(z,\lambda)W_p[\lambda,T_m(z,t)]d\lambda dz\\&=[1-R(\lambda_{\rm exc})]\left\{\int_0^\infty dz\int_{\lambda_1}^{\lambda_2}\mu_{\rm IR}(\lambda)e^{-\mu_{\rm IR}(\lambda)z}W_p(\lambda,T_0)d\lambda\right\}\\&\quad+[1-R(\lambda_{\rm exc})]\left\{\int_0^\infty dz\int_{\lambda_1}^{\lambda_2}\mu_{\rm IR}(\lambda)e^{-\mu_{\rm IR}(\lambda)z}\Delta W_p[\lambda,T_m(z,t)]d\lambda\right\}\equiv Q_0(\lambda_1,\lambda_2)+\Delta Q(t;\lambda_1,\lambda_2),\end{aligned}\tag{3}$$

where $[\lambda_1,\lambda_2]$ is the spectral (collection) bandwidth of the IR detector, $\mu_{\rm IR}(\lambda)$ is the IR absorption (emission) coefficient of the medium, $R(\lambda_{\rm exc})$ is the reflection coefficient of the medium at excitation wavelength $\lambda_{\rm exc}$, $Q_0(\lambda_1,\lambda_2)$ is the power of thermal (mid-) IR radiation emitted (absorbed) by the semi-infinite medium at thermal equilibrium at temperature T_0, and $\Delta Q(t;\lambda_1,\lambda_2)$ is the radiation power increase due to the temperature transient. For synchronous lock-in detection, only $\Delta Q(t;\lambda_1,\lambda_2)$ will be of interest.

Let

$$\bar{\mu}_{\rm IR}=\frac{\int_{\lambda_1}^{\lambda_2}W_p(\lambda,T_0)\mu_{\rm IR}(\lambda)d\lambda}{\int_{\lambda_1}^{\lambda_2}W_p(\lambda,T_0)d\lambda},$$

the spectrally weighted IR absorption (emission) coefficient for homogeneous absorbers (in practice, $\bar{\mu}_{\rm IR}$ will be a fitting parameter to experimental data). Neglecting the reflected fraction of the excitation beam from the surface, the IR thermophotonic emissive signal increase upon switching on the laser beam is spectral-bandwidth averaged:

$$\Delta Q(t)=K(\lambda_1,\lambda_2)\bar{\mu}_{\rm IR}\int_0^\infty e^{-\bar{\mu}_{\rm IR}z}\Delta T_m(z,t)dz,\tag{4a}$$

with

$$K(\lambda_1,\lambda_2)\equiv\frac{hc}{kT_0^2}\int_{\lambda_1}^{\lambda_2}\frac{W_p(\lambda,T_0)d\lambda}{\lambda[\exp(hc/\lambda k_B T_0)-1]}.\tag{4b}$$

To quantify the WM-DPTR signal generation, an expression for the optically induced temperature space and time distribution $\Delta T_m(z,t)$ will be developed.

B. Photothermal temperature field from rectangular-pulse excitation

The temperature field generated from rectangular-wave optical excitation and absorption by an analyte is dealt with in two steps: First we find $\Delta T_m(z,t)$ of a temporally impulsive excitation, and then we derive the rectangular-pulse response from the impulse response through convolution.

The photothermal impulse response to an instantaneous optical pulse of the Dirac $\delta(t)$ type and intensity I_0 [W m^{-2}] can be found. It generates a thermal power density depth profile in the medium

$$F(z,t)=I_0\mu_e e^{-\mu_e z}\delta(t);\quad 0\leqslant z<\infty,\tag{5}$$

subject to the adiabatic boundary condition

$$\left.\frac{\partial T(z,t)}{\partial z}\right|_{z=0}=0,\tag{6}$$

reflecting the fluid-air interface, where μ_e is the absorption coefficient of the medium at the excitation wavelength:

$$\mu_e\equiv\mu(\lambda_{\rm exc}).$$

The space- and time-dependent temperature field generated by the boundary value problem of Eqs. (5) and (6) can be derived using the Green function for the system, $G(z,t/z_0,t_0)$:

$$\begin{aligned}T_m(z,t)&=\frac{I_0\mu_e\alpha}{k}\int_0^{t^+}\delta(t_0)dt_0\int_0^\infty G(z,t|z_0,t_0)e^{-\mu_e z_0}dz_0\\&=\frac{I_0\mu_e\alpha}{k}\int_0^\infty G(z,t|z_0,0)e^{-\mu_e z_0}dz_0,\end{aligned}\tag{7}$$

where α is the thermal diffusivity and k is the thermal conductivity of the medium.

Using the Green function method with

$$\begin{aligned}&\frac{\partial^2}{\partial z^2}G(z,t|z_0,t_0)-\frac{1}{\alpha}\frac{\partial}{\partial t}G(z,t|z_0,t_0)\\&\quad=-\frac{1}{\alpha}\delta(z-z_0)\delta(t-t_0),\end{aligned}\tag{8}$$

subject to

$$\frac{\partial}{\partial z}G(z,t|z_0,t_0)|_{z=0}=0,\tag{9}$$

yields

$$G(z,t|z_0,t_0) = \frac{1}{2\sqrt{\pi\alpha(t-t_0)}}\left[e^{-(z-z_0)^2/4\alpha(t-t_0)} + e^{-(z+z_0)^2/4\alpha(t-t_0)}\right]H(t-t_0), \quad (10)$$

where $H(t-t_0)$ is the Heaviside function defined as

$$H(t-a) = \begin{cases} 0, & t < a \\ 1, & t > a \end{cases}. \quad (11)$$

From Eqs. (7) and (10) the temperature (photothermal) impulse response becomes

$$T_m(z,t) = \frac{I_0\sqrt{\alpha}\mu_e}{2k\sqrt{\pi t}}\int_0^\infty \left[e^{-(z-z_0)^2/4\alpha t} + e^{-(z+z_0)^2/4\alpha t}\right]e^{-\mu_e z_0}dz_0$$
$$= \frac{I_0\alpha\mu_e}{2k}\left\{e^{-\mu_e z}\operatorname{erfc}\left(\sqrt{\frac{t}{\tau_t}} - \frac{z}{2\sqrt{\alpha t}}\right) + e^{\mu_e z}\operatorname{erfc}\left(\sqrt{\frac{t}{\tau_t}} + \frac{z}{2\sqrt{\alpha t}}\right)\right\}e^{t/\tau_t}, \quad (12)$$

where $\operatorname{erfc}(y) = \frac{2}{\sqrt{\pi}}\int_0^\infty e^{-x^2}dx$, and $\tau_t \equiv \frac{1}{\mu_e^2\alpha}$ is a photothermal time constant indicating heat conduction in the photoexcited medium from a distance equal to the optical absorption depth. The temperature rise is $\Delta T_m(z,t) = T_m(z,t) - T_0$; however, the constant background temperature T_0 will not be part of the lock-in detection scheme, so it can be neglected: $\Delta T_m(z,t) = T_m(z,t)$.

For a rectangular finite optical pulse $I(t)$ we let

$$I(t) = I_0\begin{cases} 1; & 0 \leqslant t \leqslant \tau_p \\ 0; & \tau_p < t < \tau_0 \end{cases}, \quad (13)$$

where τ_p is the pulse duration and τ_0 is the pulse repetition period.

The temperature transient can be expressed as a convolution integral of the photothermal impulse response.

For $0 < t \leqslant \tau_p$, we obtain

$$\Delta T_{m1}(z,t) = \int_0^t I(\tau)\Delta T_m(z,t-\tau)d\tau = I_0\int_0^t \Delta T_m(z,t-\tau)d\tau; \quad (14)$$

Using Eq. (12) yields, after some manipulation,

$$\Delta T_{m1}(z,t) = \frac{I_0\alpha\mu_e}{2k}\left\{\begin{array}{l} e^{-\mu_e z}e^{t/\tau_t}\int_0^t e^{-\tau/\tau_t}\operatorname{erfc}\left[\sqrt{\frac{t-\tau}{\tau_t}} - \sqrt{\frac{z}{2\sqrt{\alpha(t-\tau)}}}\right]d\tau \\ +e^{\mu_e z}e^{t/\tau_t}\int_0^t e^{-\tau/\tau_t}\operatorname{erfc}\left[\sqrt{\frac{t-\tau}{\tau_t}} + \sqrt{\frac{z}{2\sqrt{\alpha(t-\tau)}}}\right]d\tau \end{array}\right\}. \quad (15)$$

For $t \geqslant \tau_p$:

$$\Delta T_{m2}(z,t) = I_0\int_0^{\tau_p}\Delta T_m(z,t-\tau)d\tau. \quad (16)$$

Carrying out the integration gives

$$\Delta T_{m2}(z,t) = \frac{I_0\alpha\mu_e}{2k}\left\{\begin{array}{l} e^{-\mu_e z}e^{t/\tau_t}\int_0^{\tau_p} e^{-\tau/\tau_t}\operatorname{erfc}\left(\sqrt{\frac{t-\tau}{\tau_t}} - \frac{z}{2\sqrt{\alpha(t-\tau)}}\right)d\tau \\ +e^{\mu_e z}e^{t/\tau_t}\int_0^{\tau_p} e^{-\tau/\tau_t}\operatorname{erfc}\left(\sqrt{\frac{t-\tau}{\tau_t}} + \frac{z}{2\sqrt{\alpha(t-\tau)}}\right)d\tau \end{array}\right\}. \quad (17)$$

It can be shown that

$$\Delta T_{m2}(z,t) = \Delta T_{m1}(z,t) - \Delta T_{m1}(z,t-\tau_p), \quad (18)$$

with $\Delta T_{m1}(z,t)$ given by Eq. (15)

C. WM-DPTR signal

From Eqs. (4) and (15), the PTR response to a rectangular optical pulse of duration $0 \leqslant t \leqslant \tau_p$ can be written as

$$\Delta Q(t) = K(\lambda_1,\lambda_2)\bar{\mu}_{\mathrm{IR}}\int_0^\infty e^{-\bar{\mu}_{\mathrm{IR}}z}\Delta T_m(z,t)dz$$
$$= \frac{I_0\alpha\mu_e\bar{\mu}_{\mathrm{IR}}}{2k}K(\lambda_1,\lambda_2)\tau_t\left\{\begin{array}{l} \frac{1}{\bar{\mu}_{\mathrm{IR}}+\mu_e}\left[W\left(\sqrt{\frac{t}{\tau_t}}\right) + W\left(\sqrt{\frac{t}{\tau_{\mathrm{IR}}}}\right) - 2\right] \\ +\frac{1}{\bar{\mu}_{\mathrm{IR}}-\mu_e}\left[W\left(\sqrt{\frac{t}{\tau_t}}\right) - W\left(\sqrt{\frac{t}{\tau_{\mathrm{IR}}}}\right)\right] \\ +\frac{2}{\bar{\mu}_{\mathrm{IR}}}\left\{2\sqrt{\frac{t}{\pi\tau_t}} - \sqrt{\frac{\tau_{\mathrm{IR}}}{\tau_t}}\left[1 - W\left(\sqrt{\frac{t}{\tau_{\mathrm{IR}}}}\right)\right]\right\} \end{array}\right\}, \quad (19)$$

where $W(x) \equiv e^{x^2}\operatorname{erfc}(x)$ and $\tau_{\mathrm{IR}} \equiv \frac{1}{\alpha\bar{\mu}_{\mathrm{IR}}^2}$ is a photothermal time constant indicating conductive heat transfer from a length equal to the mean infrared optical absorption depth, $1/\bar{\mu}_{\mathrm{IR}}$. The PTR response for $t \geqslant \tau_p$ becomes

$$\Delta Q(t \geqslant \tau_p) = \Delta Q(t) - \Delta Q(t-\tau_p). \quad (20)$$

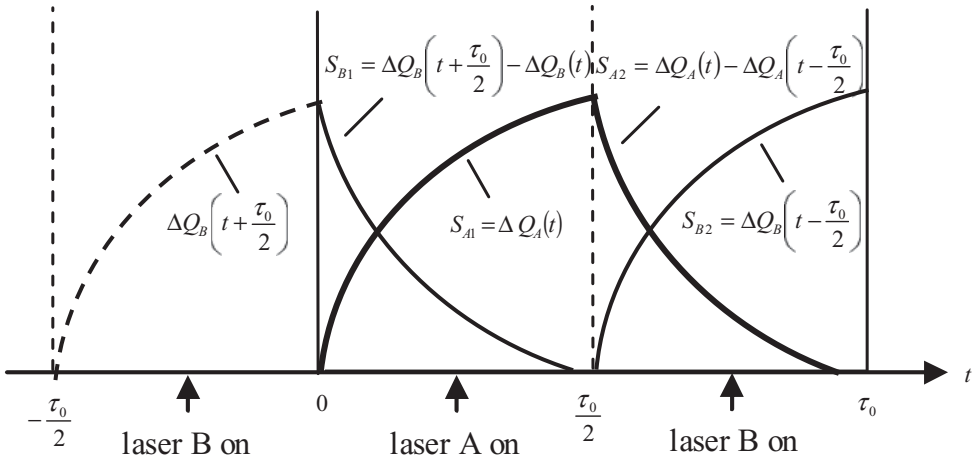

FIG. 1. PTR signals $S_A(t)$ and $S_B(t)$ from two out-of-phase square-wave excitations at 50 Hz. $S_A = S_{A1} + S_{A2}$, $S_B = S_{B1} + S_{B2}$.

Now the WM-DPTR signal from a square-wave-excited medium may be derived. For DPTR with lock-in detection, we set $\tau_p = \tau_0/2$, where τ_0 is the repetition period of the pulse. Let $\Delta Q(t) \equiv \Delta Q_A(t)$ in Eq. (19), the subscript denoting excitation due to laser A. During the cutoff period $\tau_0/2 \leqslant t \leqslant \tau_0$, laser B is turned on and generates DPTR response $\Delta Q_B(t)$. Equation (19) can be generalized to express the differential PTR signal generated by each of the laser sources A and B:

$$S_j(t) = \Delta Q_j(t) = \left[\frac{\bar{\mu}_{\rm IR} K(\lambda_1,\lambda_2)\alpha}{2k}\right] I_{0j}\mu_{ej}\tau_{tj} \left\{ \begin{array}{l} \frac{1}{\bar{\mu}_{\rm IR}+\mu_{ej}}\left[W\left(\sqrt{\frac{t}{\tau_{tj}}}\right) + W\left(\sqrt{\frac{t}{\tau_{\rm IR}}}\right) - 2\right] \\ +\frac{1}{\bar{\mu}_{\rm IR}-\mu_{ej}}\left[W\left(\sqrt{\frac{t}{\tau_{tj}}}\right) - W\left(\sqrt{\frac{t}{\tau_{\rm IR}}}\right)\right] \\ +\frac{2}{\bar{\mu}_{\rm IR}}\left\{2\sqrt{\frac{t}{\pi\tau_{tj}}} - \sqrt{\frac{\tau_{\rm IR}}{\tau_{tj}}}\left[1 - W\left(\sqrt{\frac{t}{\tau_{\rm IR}}}\right)\right]\right\} \end{array} \right\}; \quad j = A,B. \tag{21}$$

Over the full period $0 \leqslant t \leqslant \tau_0$ the sequence of photothermal responses is as follows:

$$S_{AB}(t) = \left\{ \begin{array}{ll} \Delta Q_A(t); & 0 \leqslant t \leqslant \tau_p \quad \text{(laser A on; laser B off)} \\ \Delta Q_A(t) - \Delta Q_A\left(t-\frac{\tau_p}{2}\right) + \Delta Q_B\left(t-\frac{\tau_0}{2}\right); & \frac{\tau_0}{2} \leqslant t \leqslant \tau_0 \quad \text{(laser A off; laser B on)} \end{array} \right. . \tag{22}$$

Symbolically, Eq. (22) can be written as

$$S_{AB}(t) = \Delta Q_A(t)H(t) - \Delta Q_A\left(t-\frac{\tau_0}{2}\right)H\left(t-\frac{\tau_0}{2}\right) + \Delta Q_B\left(t-\frac{\tau_0}{2}\right)H\left(t-\frac{\tau_0}{2}\right); \quad 0 \leqslant t \leqslant \tau_0. \tag{23}$$

Equation (22) does not take into account any contributions from the decaying photothermal transient of the period immediately prior to the current period commencing at $t = 0$. Therefore, the decaying transient from laser B from the period $-\tau_0 \leqslant t \leqslant 0$ should be added to the measured PTR signal as it overlaps into the $0 \leqslant t \leqslant \tau_0$ period (Fig. 1). Equation (23) can be complemented with this contribution as follows:

$$S_{AB}(t) = \left\{ \begin{array}{l} \Delta Q_A(t)H(t) - \Delta Q_A\left(t-\frac{\tau_0}{2}\right)H\left(t-\frac{\tau_0}{2}\right) \\ +\Delta Q_B\left(t-\frac{\tau_0}{2}\right)H\left(t-\frac{\tau_0}{2}\right) + \Delta Q_B\left(t+\frac{\tau_0}{2}\right) - \Delta Q_B(t); \end{array} \right. \quad 0 \leqslant t \leqslant \tau_0. \tag{24}$$

If the transient decays are slow, then the measured DPTR signal should include contributions over several prior periods. The complete set of signal contributions from decaying photothermal transients from earlier periods $t < 0$ is (with self-explanatory subscripts)

$$S_{AB0}(t) \equiv S_0(t) = \left\{ \begin{array}{l} \Delta Q_A(t)H(t) - \Delta Q_A\left(t-\frac{\tau_0}{2}\right)H\left(t-\frac{\tau_0}{2}\right) \\ +\Delta Q_B\left(t-\frac{\tau_0}{2}\right)H\left(t-\frac{\tau_0}{2}\right) \end{array} \right. \quad 0 \leqslant t \leqslant \tau_0;$$

$$S_{AB-1}(t) = \left\{ \begin{array}{l} \Delta Q_A(t+\tau_0)H(t+\tau_0) - \Delta Q_A\left(t+\frac{\tau_0}{2}\right)H\left(t+\frac{\tau_0}{2}\right) \\ +\Delta Q_B\left(t+\frac{\tau_0}{2}\right)H\left(t+\frac{\tau_0}{2}\right) - \Delta Q_B(t)H(t) \end{array} \right. \quad -\tau_0 \leqslant t \leqslant 0;$$

$$\vdots$$

$$S_{AB-N}(t) = \left\{ \begin{array}{l} \Delta Q_A(t+N\tau_0)H(t+N\tau_0) - \Delta Q_A\left[t+\left(N-\frac{1}{2}\right)\tau_0\right]H\left[t+\left(N-\frac{1}{2}\right)\tau_0\right] \\ +\Delta Q_B\left[t+\left(N-\frac{1}{2}\right)\tau_0\right]H\left[t+\left(N-\frac{1}{2}\right)\tau_0\right] \\ -\Delta Q_B\left[t+(N-1)\tau_0\right]H\left[t+(N-1)\tau_0\right]\mathrm{h}_{N,1} \end{array} \right. \quad -N\tau_0 \leqslant t \leqslant -(N+1)\tau_0;$$

where

$$h_{N,1} = \begin{cases} 1; & N \geqslant 1 \\ 0; & N = 0 \end{cases}. \tag{25a}$$

Finally, the measured total DPTR signal is

$$S_{AB}(t) = \sum_{N=0}^{\infty} S_{AB-N}(t). \tag{25b}$$

The lock-in detected signal is the Fourier transform of the WM-DPTR signal in Eq. (25) at the fundamental frequency $\omega_0 = 2\pi/\tau_0$. The demodulated signal is expressed as in-phase $\Delta S_{IP}(\omega_0)$ and quadrature $\Delta S_Q(\omega_0)$ [14]:

$$\begin{aligned} \Delta S_{IP}(\omega_0) &= \frac{2}{\pi} b_1(\omega_0), \\ \Delta S_Q(\omega_0) &= -\frac{2}{\pi} a_1(\omega_0), \end{aligned} \tag{26}$$

with

$$\begin{bmatrix} a_1(\omega_0) \\ b_1(\omega_0) \end{bmatrix} = \frac{\omega_0}{\pi} \int_0^{\tau_0} S_{AB}(t) \begin{bmatrix} \cos(\omega_0 t) \\ \sin(\omega_0 t) \end{bmatrix} dt. \tag{27}$$

Normally, the demodulated WM-DPTR signal is described as amplitude A and phase P:

$$\begin{aligned} A &= \sqrt{\Delta S_{IP}^2 + \Delta S_Q^2}, \\ P &= \tan^{-1}\left(\frac{\Delta S_Q}{\Delta S_{IP}}\right). \end{aligned} \tag{28}$$

D. WM-DPTR analyte detection

The analyte sensing capability of the WM-DPTR method is rooted in the optical and thermal property (absorption coefficient μ_e and thermal effusivity $e = k/\sqrt{\alpha}$) changes of a liquid sample with analyte concentration, which are also the basis for conventional, single-ended optical and thermal-wave diagnostic methods, respectively. However, purely optical methods (such as transmission measurements) and purely thermal-wave methods (thermal effusivity measurements) are much less sensitive than photothermal methods because the latter are based on optical and thermal property change interdependence, which acts cooperatively to enhance the sensitivity of the method. Additional sensitivity to interrelated optical and thermal property changes can be achieved by introducing differential photothermal methods, such as WM-DPTR. The thermal effusivity change due to analyte concentration change acts as an amplifying factor for the optical absorption coefficient change. This is very important because optical changes add chromophore selectivity to WM-DPTR, whereas thermal changes alone are not selective at a molecular level. The amplification of the WM-DPTR signal resulting from the optical and thermal interdependence in the presence of an analyte in a liquid medium (e.g., water) can be physically understood as follows: Tuning the IR excitation wavelength λ_A to, or near, the peak of an absorption band of the analyte, and wavelength λ_B at, or near, the absorption base line, a change in analyte concentration changes the optical absorption depth $1/\mu_{eA}$, while$1/\mu_{eB}$ remains unchanged. The resulting optical absorption and nonradiative conversion at the two wavelengths then generates proportional changes in thermal distributions depthwise in the medium (they shift the photothermal-wave centroid with changing μ_{eA}). The heat conducted away from the surface and subsurface locations in the medium does so at a rate strongly dependent on the thermal transport properties (effusivity and diffusivity). These properties also change with analyte concentration and this fact acts as a compounding amplification factor to the

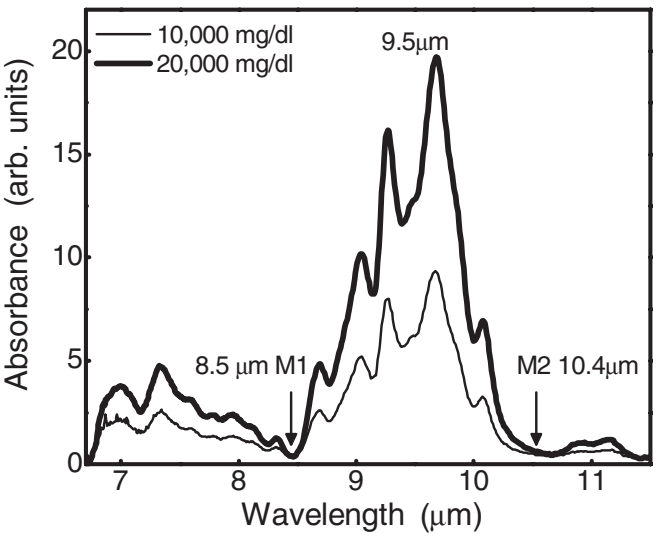

FIG. 2. FTIR glucose absorption spectra in the MIR range from aqueous glucose solutions with water absorption base line subtracted. The glucose concentrations are 10 000 mg/dl (dotted line) and 20 000 mg/dl (solid line). M1 and M2 indicate absorption-band minima on both sides of the maximum.

TABLE I. Optical and thermal property changes with glucose concentration C_g (0–300 mg/dl) in glucose aqueous solutions. μ_{eB}, absorption coefficient at λ_B (10.4 μm), is 739.51 cm^{-1} for all C_g. μ_{eA} is absorption coefficient at λ_A (9.5 μm), k thermal conductivity, α thermal diffusivity, e thermal effusivity.

C_g (mg/dl)	μ_{eA} (1/cm)	k (10^{-3} W/cm K)	α (10^{-3} cm^2/s)	e (10^{-1} W s$^{1/2}$/m^2 K)
0	531.1	6.010	1.455	1.57570
20	531.9	6.009	1.454	1.57567
40	532.8	6.008	1.453	1.57595
60	533.6	6.007	1.452	1.57653
80	534.5	6.006	1.450	1.57741
100	535.3	6.005	1.447	1.57859
120	536.1	6.004	1.444	1.58008
140	537.0	6.003	1.440	1.58187
160	537.8	6.002	1.436	1.58395
180	538.7	6.001	1.431	1.58634
200	539.5	6.000	1.426	1.58902
220	540.3	5.999	1.420	1.59200
240	541.2	5.998	1.414	1.59527
260	542.0	5.997	1.407	1.59883
280	542.9	5.996	1.400	1.60268
300	543.7	5.995	1.392	1.60682

optical asymmetry at λ_A and λ_B with changing analyte concentration.

III. GLUCOSE-IN-WATER DETECTION SIMULATIONS

Based on the WM-DPTR theory, glucose detection was simulated using the MATLAB program and validated with a WM-DPTR experimental system. In the simulations, water-glucose solutions with glucose concentration 0–300 mg/dl, covering the full human blood range from hypoglycemia (below 70 mg/dl), to normal (80–140 mg/dl), to hyperglycemia (above 140 mg/dl), were considered to be photothermally excited using two out-of-phase laser beams of wavelength $\lambda_{eA} = 9.5\ \mu$m and $\lambda_{eB} = 10.4\ \mu$m coincident with peak and base line of the major glucose absorption band in the MIR (Fig. 2). The glucose spectrum was obtained using our own water solutions. The detection band $[\lambda_1,\lambda_2]$ was set to 2–5 μm, consistent with today's midinfrared photodiode detectors. Since there is no major glucose absorption band in this range, the IR absorption (emission) coefficient $\mu_{\mathrm{IR}}(\lambda)$ of the solvent was replaced by that of water. The optical and thermal properties of water with different glucose concentration C_g are listed in Table I. The absorption coefficient μ_{eA} was calculated based on Ref. [11] while μ_{eB} does not change with C_g. The thermal conductivity k was calculated from a simple equation [15]: $k = k_w + aC_g$, where k_w is the thermal conductivity of water [W/mK] and $a = -0.00162$ [(W/mK)/(mg/dl)]. The thermal diffusivity α was calculated from $\alpha = k/\rho c_p$, where ρ and c_p are the density and specific heat of the solution, respectively [16,17]. The modulation frequency $f(=1/\tau_0)$ was set at 10, 50, and 150 Hz. There are two important input parameters in the simulations: amplitude ratio R and phase shift ΔP. Amplitude ratio R is defined as the ratio of pure water PTR amplitudes generated from laser A and laser B alone: $R = A_{Aw}/A_{Bw}$. $R$is normally set in the neighborhood of 1 by adjusting the laser intensity ratio $R_I = I_{0A}/I_{0B}$. Phase shift ΔP is defined as the phase difference between water PTR phases generated from lasers A and B alone: $\Delta P = P_{Aw} - P_{Bw}$. The phase shift is normally set around 180° by adjusting the modulated laser intensity phase shift $\Delta P_I = P_{IA} - P_{IB}$. Specifically, a time lead or delay Δt was added to the PTR signal from laser B: $S_B = S_B(t + \Delta t)$. It should be noted that $R \neq R_I$, $\Delta P \neq \Delta P_I$. Output signals were calculated both as transient wave forms $S(t)$ and lock-in demodulated amplitudes and phases $A(f)$ and $P(f)$. For the purpose of comparison, the outputs include both single-ended

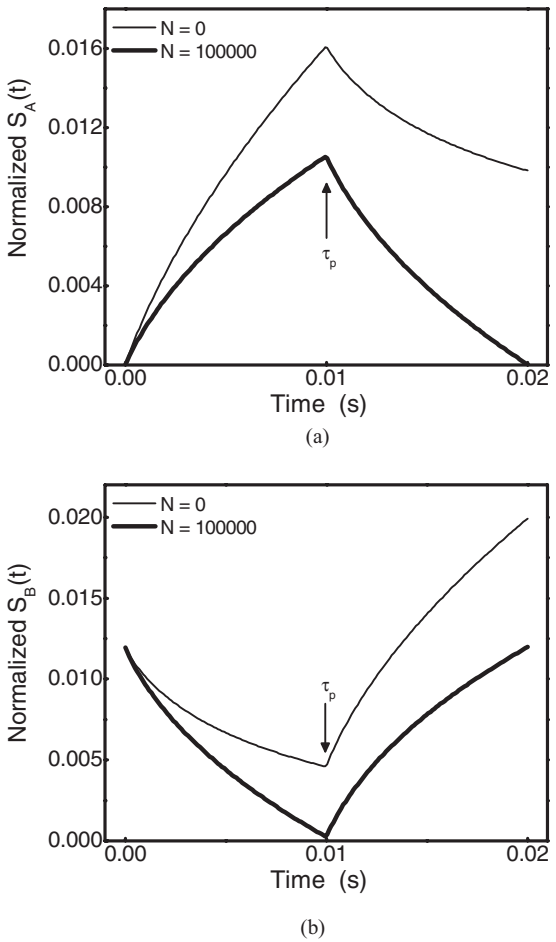

FIG. 3. Effect of accumulation number N on PTR signal wave forms $S_A(t)$ (a) and $S_B(t)$ (b) at 50 Hz with laser intensity ratio $R_I = 1$, laser phase shift $\Delta P_I = 180°$. The values of N are shown in the inset.

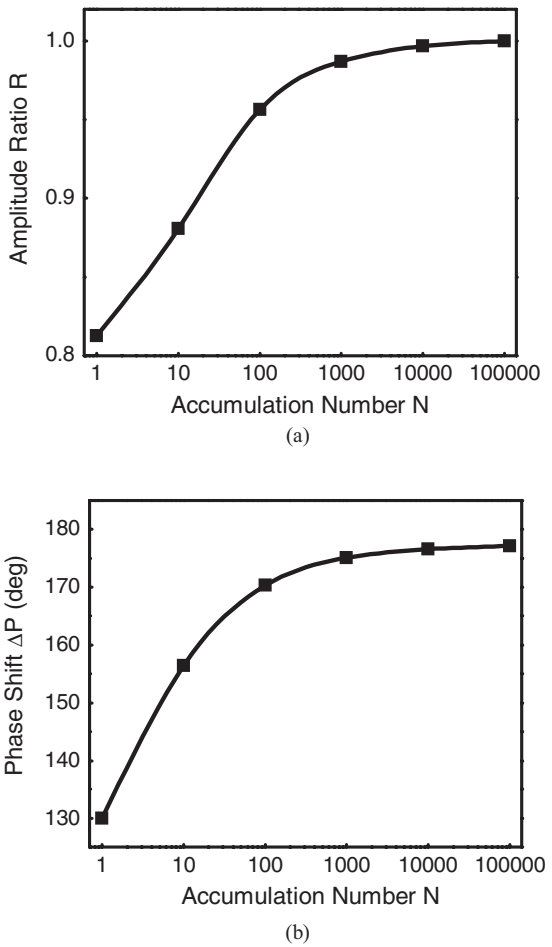

FIG. 4. Effect of accumulation number on lock-in demodulated signals at 50 Hz with laser intensity ratio $R_I = 1$ and phase shift $\Delta P_I = 180°$: (a) Amplitude ratio R; (b) phase shift ΔP.

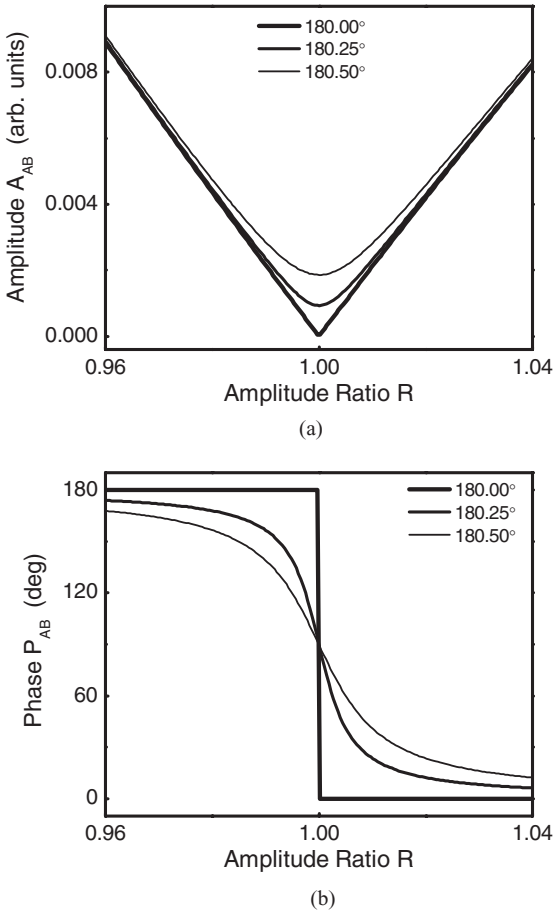

FIG. 5. Phase shift effect on water base line as a function of amplitude ratio R at 50 Hz: (a) Amplitude A_{AB}; (b) phase P_{AB}. ΔP values are shown in the inset.

signals generated from a single laser ($S_A(t)$, $S_B(t)$, A_A, A_B, P_A, and P_B) and differential signals generated from both lasers ($S_{AB}(t)$, A_{AB}, and P_{AB}). The modulation frequency used in the theoretical simulation results is 50 Hz unless specified otherwise.

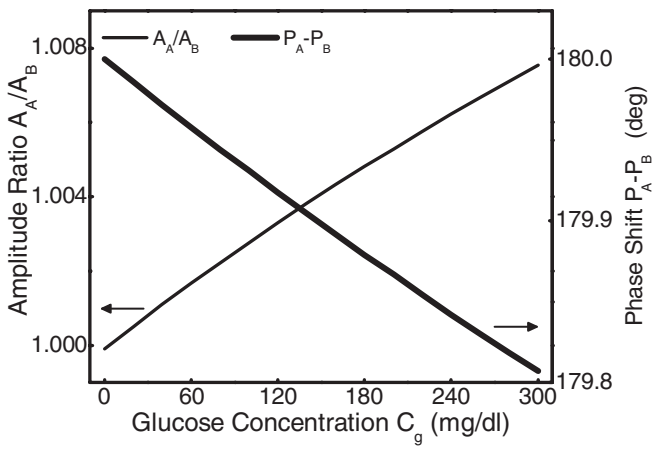

FIG. 6. Glucose (0–300 mg/dl)-induced changes in DPTR amplitude ratio A_A/A_B and phase shift $P_A - P_B$ at 50 Hz.

A. Determination of amplitude ratio R and phase shift ΔP

In the WM-DPTR method, for optimal performance the amplitude ratio and phase shift of two single PTR signals from a glucose-free liquid medium must be ∼1 and 180° (out-of-phase), respectively. It was found from simulations that the transient accumulation number (or signal settling number) N, in Eq. (25b), plays an important role in the proper determination of the amplitude ratio and the phase shift. Presented in Fig. 3 are two PTR signals $S_A(t)$, Fig. 3(a), and $S_B(t)$, Fig. 3(b), from lasers A(λ_A) and B(λ_B), respectively. The shapes of the two wave forms are strongly dependent on the settling number N which increased from 0 to 10^5. With contributions from 10^5 previous cycles, the sampled signals exhibit full decay, consistent with experimental results. The accompanying dc signal increases are not shown here because the subsequent lock-in demodulation process eliminates them. The resultant amplitude ratio and phase shift of the two demodulated signals are also N dependent, as shown in Fig. 4. With sensitivity requirements that laser intensity ratio R_I be set at 1 and phase shift ΔP_I at 180°, when N increases from 0 to 10^5, the amplitude ratio R increases from ∼0.66 to ∼1, Fig. 4(a), and the phase shift increases from ∼146° to ∼180°, Fig. 4(b). R and ΔP change greatly for $N < 100$

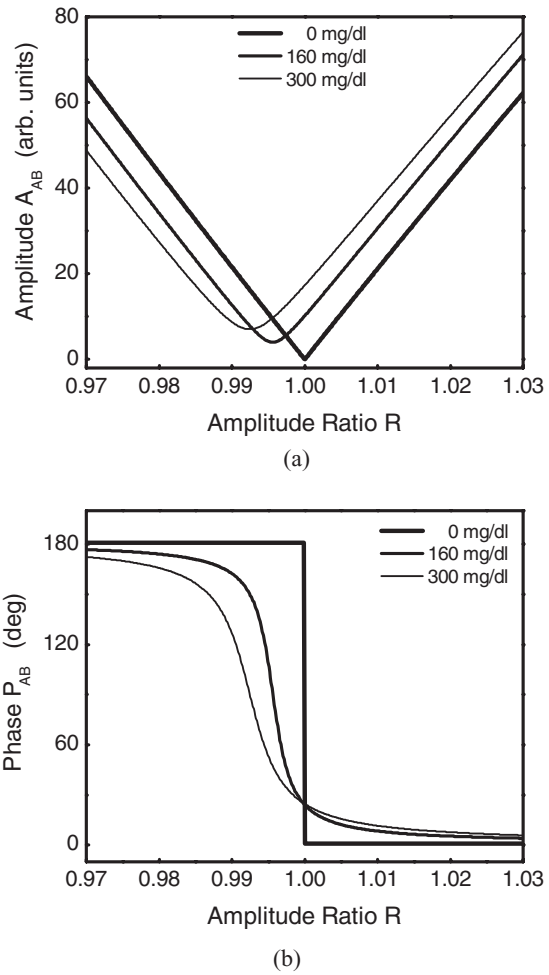

FIG. 7. Glucose-induced water base line change at 50 Hz: (a) Amplitude A_{AB}; (b) phase P_{AB}. Glucose concentrations in the 0–300 mg/dl range are shown in the inset.

and then approach saturation for $N > 1000$. To simulate our experimental measurement conditions with ~50 s settling time, N was set at 500 for 10 Hz, 2500 for 50 Hz, and 7500 for 150 Hz. The remainder between R (ΔP) and 1 (180°) was compensated through change of intensity ratio and addition of a lead time Δt to the PTR signal $S_B(t)$ in the millisecond or submillisecond level, depending on modulation frequency.

B. Water base line and glucose detection mechanism

Since human blood-range aqueous glucose solutions are water solutions with small perturbations, photothermal properties of the water base line were studied first. Figure 5 shows amplitude A_{AB} and phase P_{AB} of the water-generated WM-DPTR signal vs amplitude ratio ($R = 0.98$ to 1.04) with various phase shifts ($\Delta P = 180°$, 180.25°, and 180.5°). The amplitude at 180° phase shift, Fig. 5(a), forms a V curve, with nearly zero minimum around $R = 1$. With an increase in phase shift, the minimum of the V curve becomes rounded off and rises. These minima also occur at $R \approx 1$ where the two amplitudes A_A and A_B have similar magnitudes so they cancel each other out, or nearly so, depending on the phase shift. The closer to 180° ΔP is, the sharper and lower the minimum. The amplitude change with phase shift change increases in the neighborhood of $R \approx 1$ from both directions and becomes maximum at $R = 1$. The phase of the water signal, Fig. 5(b), takes the shape of a step function, transitioning from the single-laser PTR phase P_B to P_A (180° to 0°) around $R = 1$. With increasing phase shift, the phase transition becomes more gradual. The most affected regions (tens of degrees of change) are just below and above $R = 1$. Unlike the amplitude, there exists an unaffected region around $R = 1$ at the middle point of the transition where all the phase curves cross. Figure 5 shows that the water base line is very sensitive to phase shift change. It also demonstrates that WM-DPTR functions as a photothermal signal amplifier: A tiny change (subdegree) in the single PTR signals ($P_A - P_B$) can be amplified to tens of degrees (~90° maximum) in the DPTR signal (P_{AB}).

When glucose is added (dissolved) into pure water, the phase shift as well as the amplitude ratio will change as shown in Fig. 6. For the human blood glucose concentration range 0–300 mg/dl, the amplitude ratio A_A/A_B *increases from 1 to ~1.008* and the phase shift $P_A - P_B$ *decreases from 180° to ~179.81°*. The resultant amplitude and phase signals vs amplitude ratio R at glucose concentrations 0, 160, and 300 mg/dl are plotted in Fig. 7. As expected, the amplitude in Fig. 7(a) exhibits similar trends to Fig. 5(a): a set of V curves with minima becoming rounded off and rising as glucose concentration increases. This is so because glucose causes a phase shift deviation. However, the V curves are not symmetric

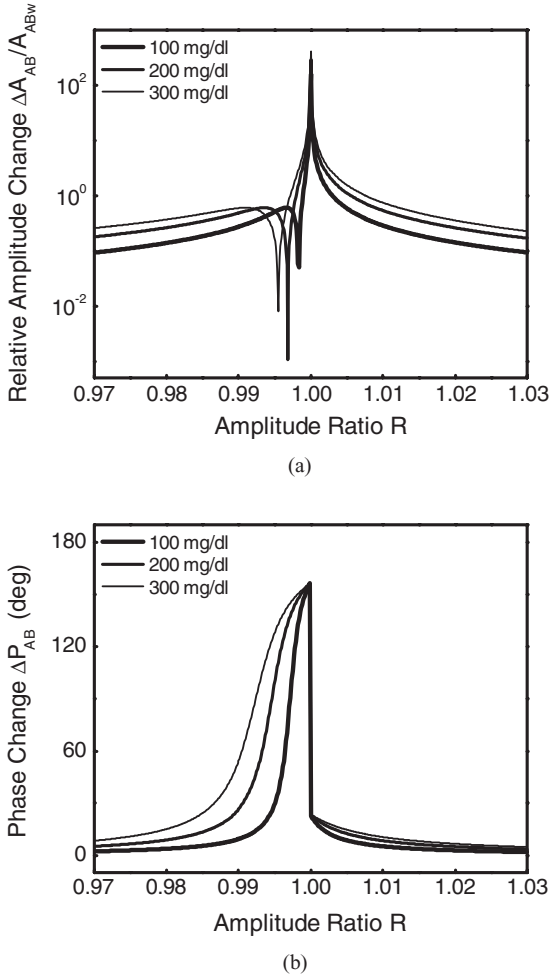

FIG. 8. Amplitude ratio R dependence of WM-DPTR signal response to various glucose concentration changes at 50 Hz: (a) Amplitude response; (b) phase response.

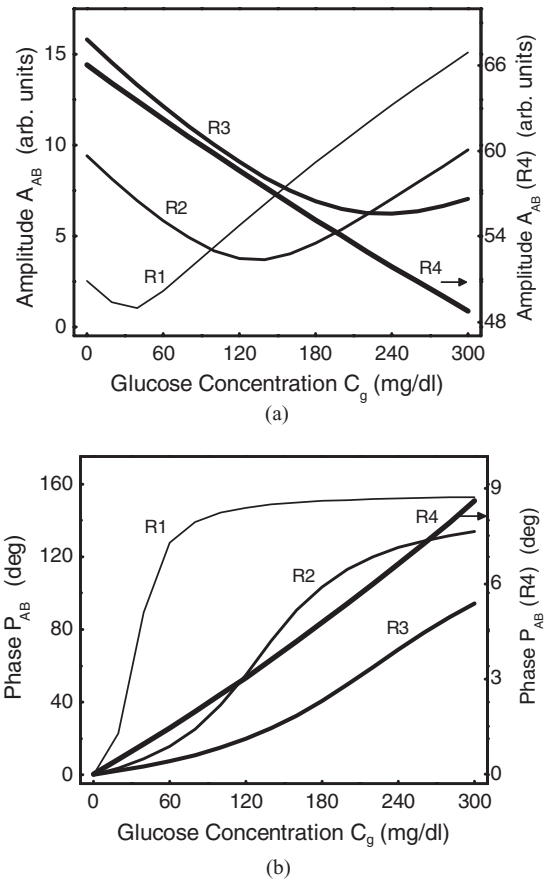

FIG. 9. Amplitude ratio R dependence of WM-DPTR signal on glucose concentration at 50 Hz: (a) Amplitude A_{AB}; (b) phase P_{AB}. $R1 = 0.999$; $R2 = 0.996$; $R3 = 0.993$; $R4 = 0.97$.

about $R = 1$ as in Fig. 5(a), with the minimum shifting toward *smaller* R with increasing concentration. This is due to the *increase* of amplitude ratio A_A/A_B with glucose concentration. The shifting of the minimum allows for a larger dynamic range in the region $R > 1$. However, the amplitude is not monotonic, exhibiting low resolution in the region $R < 1$. In Fig. 7(b) the phase also follows the same trend as in Fig. 5(b): The phase transition becomes more gradual with glucose concentration due to the phase shift deviation and its resolution is low in the region $R > 1$. The crossing point, intrinsically insensitive to glucose, is pushed down *below* the midpoint, so that the dynamic range in the region $R < 1$ increases to $\sim 157^\circ$ at the cost of shrinking dynamic range in the region $R > 1$.

Figures 7(a) and 7(b) indicate that the glucose detection sensitivity of WM-DPTR is amplitude ratio dependent and the amplitude and phase are two complementary metrics. This can be seen more clearly in Fig. 8, which shows the total relative amplitude change $\Delta A_{AB}/A_{ABw}$ ($\Delta A_{AB} = A_{AB} - A_{ABw}$, amplitude change between pure water differential signal A_{ABw} and glucose solution differential signal A_{AB}) and phase change ΔP_{AB} ($\Delta P_{AB} = P_{AB} - P_{ABw}$, phase change between pure water differential signal P_{Aw} and glucose solution differential signal P_{AB}) due to 100, 200, and 300 mg/dl glucose concentration changes against amplitude ratio R. It is shown that the glucose sensitivity of both amplitude and phase strongly depends on amplitude ratio R, peaking within an extremely narrow range. Asymmetrically broader shoulders appear *above* $R = 1$ for the amplitude and *below* $R = 1$ for the phase. Sharp dips in the amplitude appear on the *left* side ($R < 1$). In general WM-DPTR demonstrates dynamic range advantage over single-ended PTR. The latter only yields ~ 0.03 in relative amplitude change and $\sim 0.3^\circ$ in phase change for the same percentage of glucose concentration change (300 mg/dl).

WM-DPTR signals are normally nonlinear with glucose concentration and this dependence also changes with amplitude ratio R. Figure 9 presents amplitude and phase dependence on glucose concentration at four amplitude ratios $R1$–$R4$. It can be seen from the phases, Fig. 9(b), that each amplitude ratio favors a different glucose concentration range: $R1$ produces enhanced sensitivity in the low range (0–60 mg/dl), $R2$ in the medium-to-high range (60–180 mg/dl), $R3$in the high range (180–300 mg/dl), and $R4$ in the entire range, but with relatively low sensitivity. Very importantly for potential clinical applications, the amplitudes in Fig. 9(a) complement the phase sensitivity at each R value; for example, at $R1$

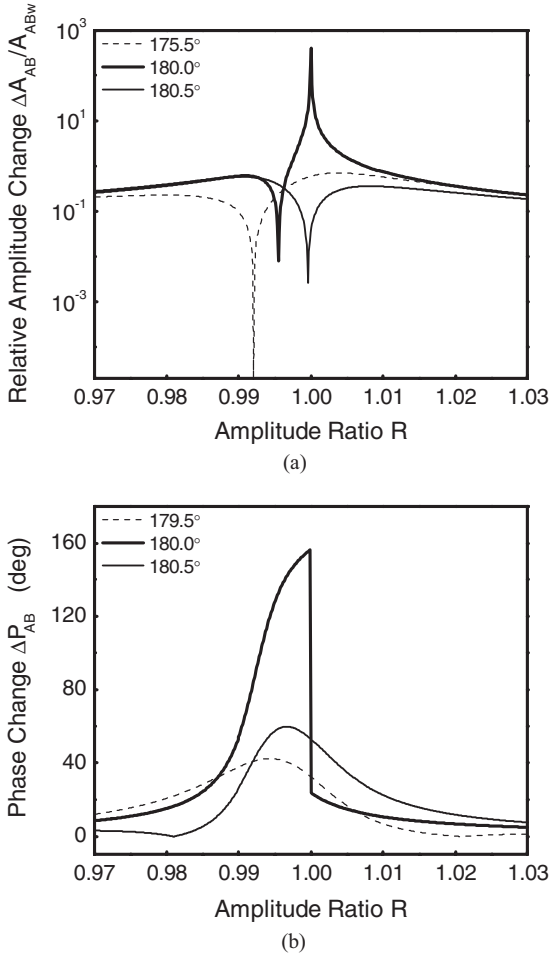

FIG. 10. Phase shift change ($\pm 0.5^\circ$) effect on glucose detection sensitivity at 50 Hz for a 300 mg/dl glucose concentration change from pure water: (a) Relative amplitude change; (b) phase change.

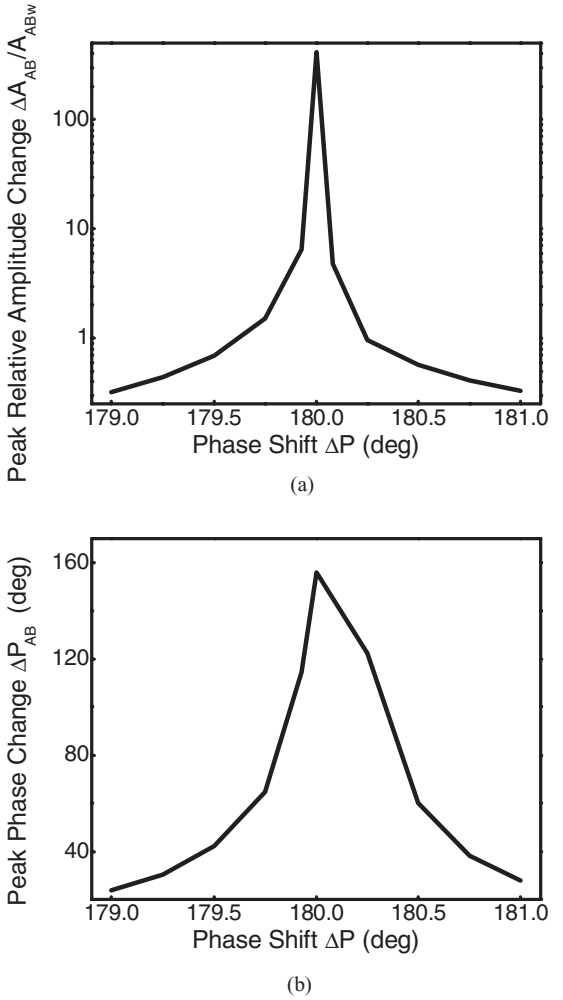

FIG. 11. Phase shift of peak glucose sensitivity (for a 300 mg/dl glucose concentration change) at 50 Hz: (a) Peak relative amplitude change; (b) peak phase change.

the amplitude exhibits high sensitivity to $C_g > 60$ mg/dl, a range where the phase is fully saturated. It is noticed that the amplitudes at $R1$, $R2$, and $R3$ are nonmonotonic over the full glucose concentration range.

C. Other effects on glucose detection sensitivity

In addition to the amplitude ratio, the glucose detection sensitivity is also affected by other factors, such as changes in water base line phase shift deviation and modulation frequency f.

Figure 10 displays three signal response curves to a 300 mg/dl glucose concentration change from pure water using different phase shifts: 179.5°, 180°, and 180.5°. For ±0.5° deviation from the 180° phase shift, peak sensitivities drop greatly: ∼99% in amplitude and 68% in phase. The peak and dip positions are also affected. The peak sensitivity change with larger phase shift deviation (±1°) is illustrated in Fig. 11. Figure 11(a) indicates that peak amplitude changes are narrow: 0.25° shift away from 180° affects amplitude peak sensitivity most strongly, whereas the shift effect on phase is broader than amplitude and essentially symmetric about $\Delta P = 180°$, Fig. 11(b). Figure 12 shows phase curves as functions of amplitude ratio for various glucose concentrations (0, 100, 200, and 300 mg/dl). The phase shift ΔP is 180.25°. The phase change region becomes steeper with increasing glucose concentration and undergoes a very sharp transition (flip-over) at *different amplitude ratios*. This is so because the phase shift *decreases* with glucose concentration as shown in Fig. 6 (where $\Delta P = 180°$, not 180.25°). For $\Delta P = 180.25°$, the phase shift approaches 180° *with increasing glucose concentration*. It should be noted that the phase flip-over, which occurs for each glucose concentration at a different amplitude ratio, may be used as a sensitive method to measure that concentration.

Figure 13 demonstrates the effects of frequency change on glucose sensitivity: The signal responses to a 300 mg/dl glucose concentration with three different modulation frequencies, 10, 50, and 150 Hz, were investigated. The figure shows

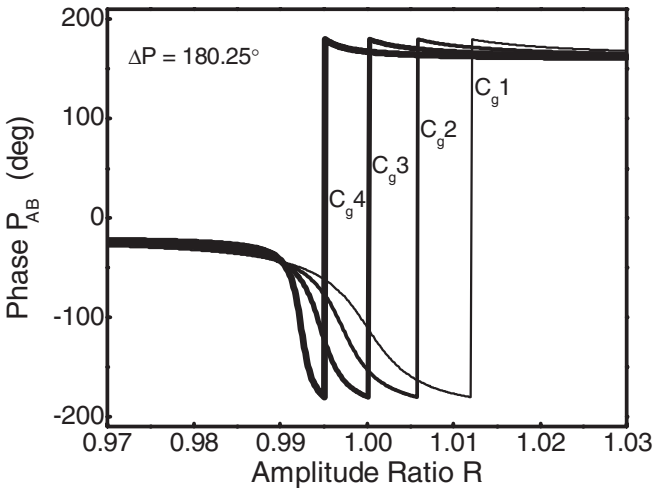

FIG. 12. Phase transitions (flip-overs) with phase shift *larger* than 180° ($\Delta P = 180.25°$). Glucose concentrations are $C_{g1} = 0$ mg/dl, $C_{g2} = 100$ mg/dl, $C_{g3} = 200$ mg/dl, $C_{g4} = 300$ mg/dl.

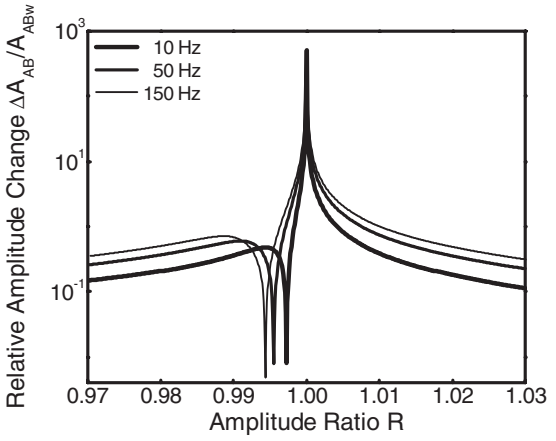

(a)

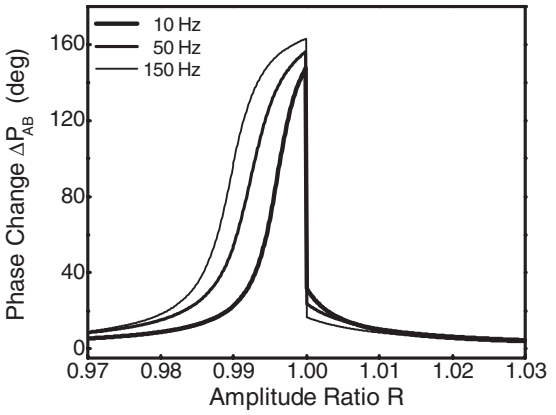

(b)

FIG. 13. The effect of frequency change on glucose sensitivity vs amplitude ratio R. (a) Relative amplitude change; (b) phase change for a 300 mg/dl glucose concentration change.

that the main peak half-width of both amplitude sensitivity, Fig. 13(a), and phase sensitivity, Fig. 13(b), around $R \sim 1$ *increases* with increasing frequency. Simulations show that the peak value of the sensitivity increases with frequency for phase and decreases for amplitude.

D. Detection configuration comparisons

The roles of optical (μ_{eA}) and thermal (α and k) properties in WM-DPTR glucose detection were studied using a comparison among four configurations: (1) α and k fixed (at water values) while μ_{eA} changes with glucose concentration, (2) μ_{eA} fixed ($\mu_{eA} = \mu_{eB}$) while α and k change, (3) μ_{eA} fixed ($\mu_{eA} \neq \mu_{eB}$) while α and k change, and (4) μ_{eA}, α, and k all change. The glucose-induced changes (0–300 mg/dl) in amplitude ratio A_A/A_B and phase shift $P_A - P_B$ are presented in Fig. 14. The amplitude ratio, Fig. 14(a), exhibits a slight *decrease* in configuration (conf.) (3), almost no change in conf. (2), and large *increases* in both confs. (1) and (4). The phase shift, Fig. 14(b), exhibits *small increases* in both confs. (2) and (3) and *large decreases* in both confs. (1) and (4). The amplitude and phase responses to a 300 mg/dl glucose concentration with the four configurations are presented in

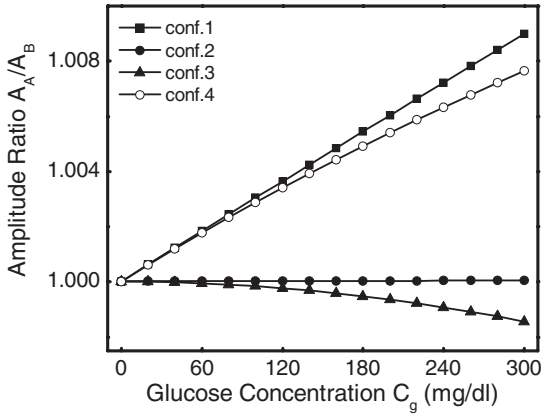

(a)

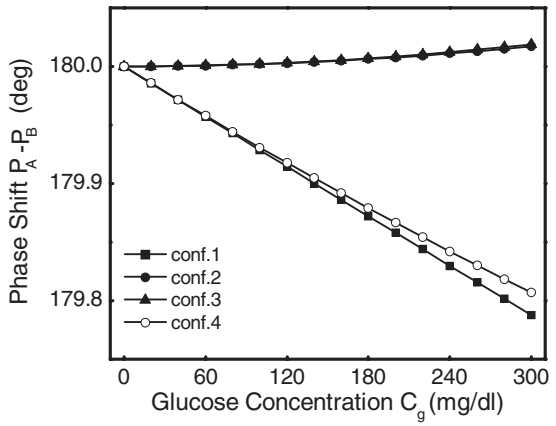

(b)

FIG. 14. Comparison of glucose-induced change in amplitude ratio (A_A/A_B) and phase shift $(P_A - P_B)$ in four hypothetical system configurations at 50 Hz. (1) Thermal properties (α, k) fixed, optical property (μ_{eA}) changes with C_g; (2) optical properties (set $\mu_{eA} = \mu_{eB}$) fixed, thermal properties (α, k) change with C_g; (3) optical properties $(\mu_{eA} \neq \mu_{eB})$ fixed, thermal properties (α, k) change with C_g; (4) both optical (μ_{eA}) and thermal (α, k) properties change with C_g.

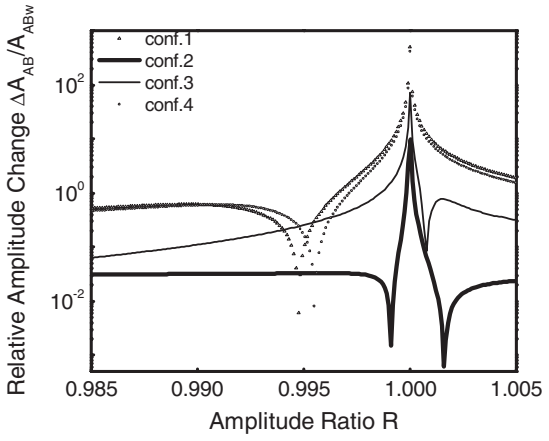

(a)

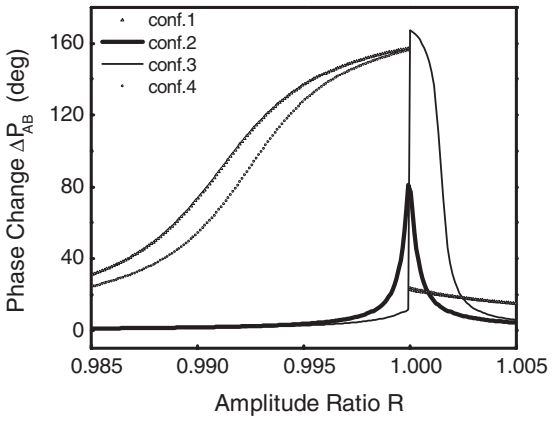

(b)

FIG. 15. Comparison of glucose sensitivity at 50 Hz for the four system configurations of Fig. 14. (a) Relative amplitude change; (b) phase change.

Fig. 15. Figure 15(a) shows that configurations (1) and (4) yield the largest responses, while configuration (2) yields the smallest response. Figure 15(b) shows that (1) and (4) have higher and wider sensitivity ranges while (2) has a lower peak and a much narrower sensitivity range. Figure 15 demonstrates that the predicted glucose sensitivity of WM-DPTR is a cooperative effect due to optical property changes as amplified by differential optical absorptions and accompanied by thermal property changes. The reason for which WM-DPTR is more sensitive in conf. (1) (changes in μ_{eA} alone) than in conf. (4) is because part of the optical-property-change-induced phase shift is canceled out by the thermal-property-change-induced phase shift. If μ_{eB} is selected to be smaller than μ_{eA}, for example, the left minimum M1 of the glucose absorption peak, Fig. 2, the glucose selectivity of μ_{eA} will be even more enhanced because the increase of μ_{eA} with glucose concentration increases the difference, which, in turn, increases glucose detection sensitivity. As can be seen in Fig. 16, selecting M1 as base line wavelength is more advantageous *because of the complementarily wider peaks in both amplitude* [Fig. 16(a)] *and phase* [wider for $R < 1$, Fig. 16(b)] *channels*.

IV. EXPERIMENTAL AND PRELIMINARY RESULTS

An experimental WM-DPTR system was developed as guided by the foregoing WM-DPTR theory, in order to measure water-glucose solutions (Fig. 17). The setup consisted of two quantum cascade lasers and a laser controller (QCL, 1101-95/104-CW-100-AC, Pranalytica, CA) emitting at wavelengths 9.5 and 10.4 μm (at the M2 base line absorption wavelength), a HgCdZnTe detector (MCZT, PVI-4TE-5, Vigo System, Poland) sensitive in the 2–5-μm spectral bandwidth, a function generator (33220A, Agilent Technologies, CA) and a lock-in amplifier (SR830, Stanford Research Systems, CA), or a digital oscilloscope (DPO 7104, Tektronix, OR). The square-wave out-of-phase modulated laser beams impinged on the sample which consisted of water and glucose and generated PTR signals. The differential signal was collected by the MCZT detector and then sent to the lock-in amplifier for demodulation, or was sent to an oscilloscope to view the wave forms. The amplitude ratio R was controlled

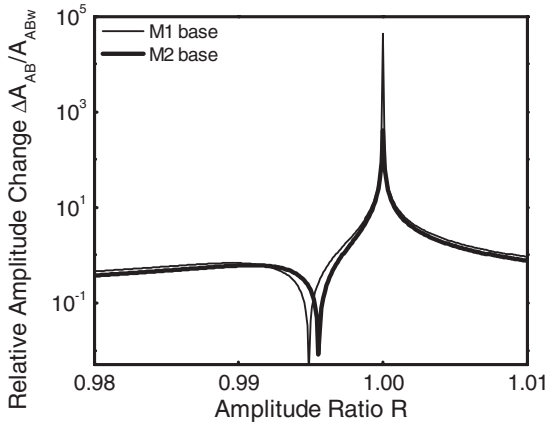

FIG. 16. Comparison of glucose sensitivity with M1 base line and M2 base line, Fig. 2, at 50 Hz under (a) relative amplitude change; (b) phase change.

by the laser controller and the phase shift ΔP was controlled by the function generator.

Figure 18 displays WM-DPTR wave forms for pure water measured by the digital phosphor oscilloscope. Although the

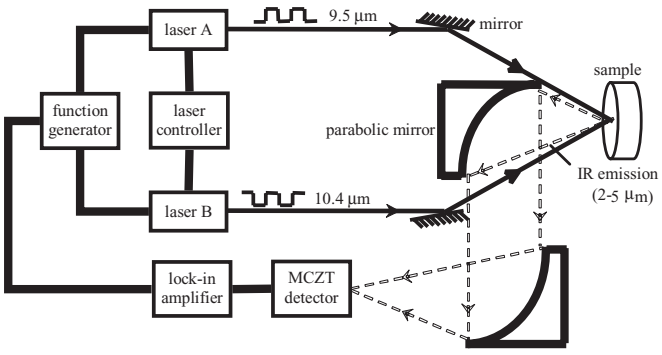

FIG. 17. (Color online) Schematic diagram of WM-DPTR system. Square-wave modulated radiation from laser A (9.5 μm) and laser B (10.4 μm) incident on the sample generates superposed IR emissions. The differential infrared photon flux is collected by the MCZT detector acting as a bandpass filter (2–5 μm, dashed line) and sent to a lock-in amplifier. The function generator controls the phase shift between the two laser beams and the laser controller controls the intensity ratio of the two lasers.

experimental data (symbols) are noisy due to low signals, they are in agreement with the theoretical best fits (lines).

Water base line measurements with the lock-in amplifier at 50 Hz at five different phase shifts (179°–181°) are presented in Fig. 19. The symbols are experimental results and the lines are theoretical fits. Parameters from the literature used in the simulations are $\alpha = 1.45 \times 10^{-3}$ cm^{2}s^{-1} [15–17], $k = 6 \times 10^{-3}$ W K^{-1}cm^{-1} [15], $I_{0A}/I_{0B} = 0.999$–1.268, $\mu_{eA} = 531.1$ cm^{-1} [18], $\mu_{eB} = 739.51$ cm^{-1} [18]. Parameters obtained from the theoretical best fits, Eq. (25b), are $\bar{\mu}_{\rm IR} = 939$ cm^{-1}, $K(\lambda_1,\lambda_2) = 0.0364$ W K^{-1}cm^{-3}, $\tau_{\rm IR} = 7.8 \times 10^{-4}$ s, $\tau_{tA} = 2.5 \times 10^{-3}$ s, $\tau_{tB} = 1.3 \times 10^{-3}$ s. For amplitude best fits in Fig. 19(a), curves obtained with ΔP of 179°, 179.5° are not presented because they almost overlap the 180.1° and 180.5° curves. The agreement between theory and experiment is excellent, especially for the phases. The relatively larger deviation in fitting the amplitude is due to the fact that amplitude is more easily influenced by other factors such as temperature and sample surface conditions.

Figure 20 shows the amplitude ratio dependence of amplitude and phase with 0 and 300 mg/dl glucose in water with a phase shift $\Delta P = 179.75°$ at 50 Hz. The symbols are measurement data and the lines are theoretical fits using Eq. (25b) with parameters from the literature $\mu_{eA} = 531.1$ (540.3) cm^{-1}

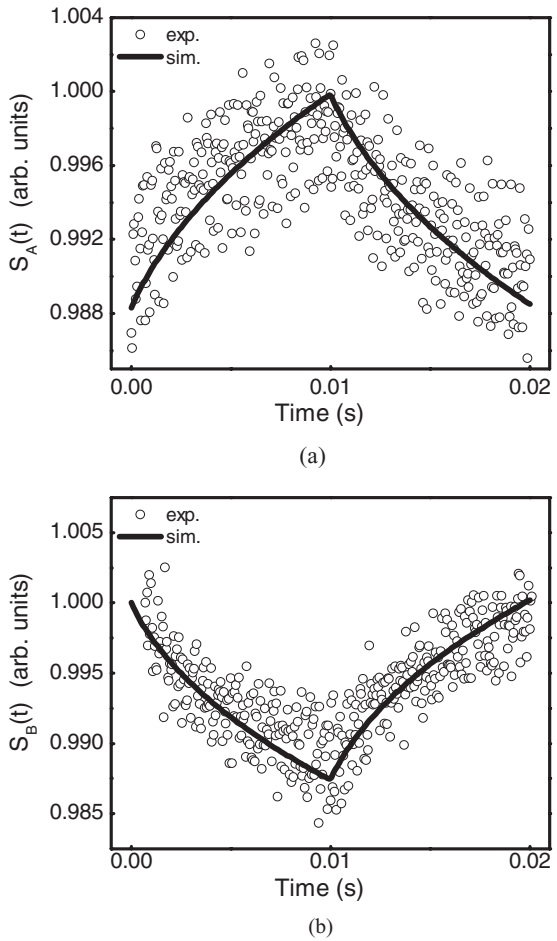

FIG. 18. Single-ended pure water PTR-response wave form traces from oscilloscope (symbols) and theory (lines) at 50 Hz. (a) $S_A(t)$; (b) $S_B(t)$.

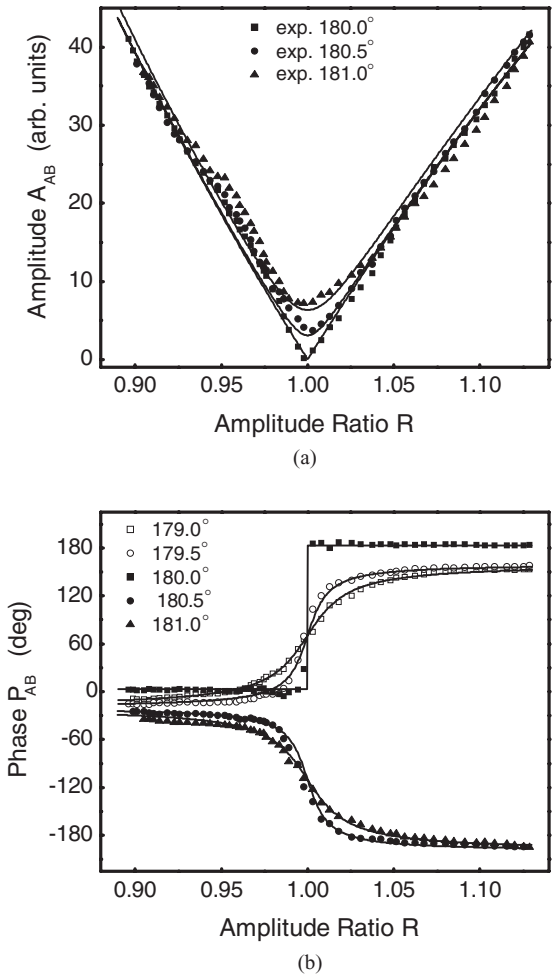

FIG. 19. Theoretical fits to WM-DPTR experimental data using pure water. (a) Amplitude A_{AB}; (b) phase P_{AB}. The symbols are measurement results and the lines are theory, Eq. (28), using Eq. (25) in the demodulation integrand of the lock-in IP and Q channels, Eq. (27).

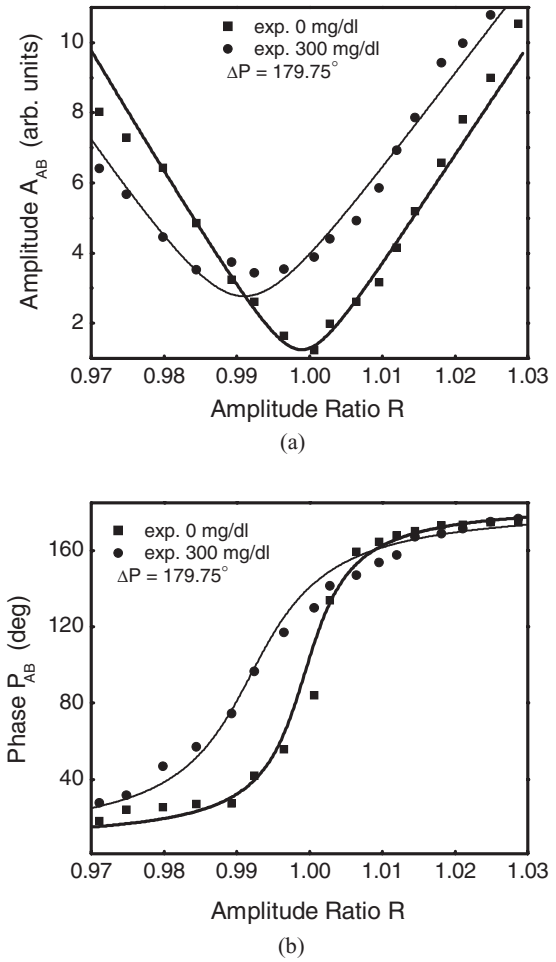

FIG. 20. Results with 0 and 300 mg/dl glucose concentration in water at 50 Hz with phase shift $\Delta P = 179.75°$. (a) Amplitude vs amplitude ratio, (b) phase vs amplitude ratio. The symbols are measurement results and the lines are theoretical best fits to Eq. (28) using Eq. (25) in the demodulation integrand of the lock-in IP and Q channels, Eq. (27).

[18], $k = 6.01 \times 10^{-3}$ (5.995×10^{-3}) W K^{-1}cm^{-1} [15]. Derived parameters from the best fits are $\bar{\mu}_{\rm IR} = 939$ cm^{-1}, $K(\lambda_1,\lambda_2) = 0.0364$ W K^{-1}cm^{-3}, $\tau_{\rm IR} = 7.8 \times 10^{-4}$ (8.15×10^{-4}) s, $\tau_{tA} = 2.437 \times 10^{-3}$ (2.430×10^{-3}) s, $\tau_{tB} = 1.287 \times 10^{-3}$ (1.345×10^{-3}) s. The values in brackets correspond to glucose solution of 300 mg/dl. It is seen that the theory fits the data very well for both amplitude, Fig. 20(a), and phase, Fig. 20(b), in the range $0.97 < R < 1.03$ where the signal-to-noise ratio is relatively high.

The amplitude ratio scans consisting of 17 data points are slow, so there might be fluctuations in the measurement results due to instrumental drift with some data points diverging from theoretical curves.

V. CONCLUSIONS

We have introduced the WM-DPTR technique, both theoretically and experimentally for noninvasive biological analyte detection, such as blood glucose monitoring. A theoretical model was developed based on differential photothermal radiometric signals from peak and base line absorptions of the mid-IR pyran ring of the glucose molecule. Model based simulations of glucose detection in aqueous phantoms in the clinically relevant range demonstrated its superior sensitivity due to cooperative photothermal amplification effects when compared with the single-ended method. The amplitude ratio and phase shift of the pure water base line were found to play a very important role in detection sensitivity. The amplitude and phase of the WM-DPTR signal act as two complementary glucose measurement channels. A third glucose concentration measurement method can be introduced if the base line phase shift is *larger* than 180°. It was found that, through proper selection of the excitation laser intensity ratio and the corresponding optimal modulation frequency, the WM-DPTR glucose measurement mode can be adjusted for maximum sensitivity to the glucose range of interest for accurate evaluation of biologically relevant glucose concentrations, from hypoglycemia to hyperglycemia. An experimental WM-DPTR system was designed and preliminary aqueous glucose solution measurement results

were obtained, yielding very-good-to-excellent fits to the theoretical model.

ACKNOWLEDGMENTS

Preliminary discussions are gratefully acknowledged with Dr. Bernard Zinman, Simon Lunenfeld Centre for Diabetes, Mount Sinai Hospital, Toronto, on future clinical diagnosis tests which led to the preliminary experimental results with glucose-water mixtures. We thank the NSERC-CIHR CHRP program, the Ontario Ministry of Research and Innovation (MRI) and the NSERC Discovery Program for financial support of this research. We are grateful to Dr. K. Patel (Pranalytica, Inc.) for helpful discussions on, and partial support of, the QCL system.

[1] M. Jones and J. M. Harrison, Diabetes Technol. Ther. **4**, 351 (2002).
[2] M. B. Davidson, in *Diabetes Mellitus—Diagnosis and Treatment*, 3rd ed. (Churchill Livingstone, New York, 1991), p. 231.
[3] S. Auxter, Clin. Chem. News **Nov.**, 5 (1996).
[4] R. McNichols and G. Coté, J. Biomed. Opt. **5**, 5 (2000).
[5] A. Tura, A. Maran, and G. Pacini, Diabetes Res. Clin. Pract. **77**, 16 (2007).
[6] *Handbook of Optical Sensing of Glucose in Biological Fluids and Tissues*, 1st ed., edited by V. V. Tuchin (CRC Press, Boca Raton, FL, 2008).
[7] C. J. Pouchert, *The Aldrich Library of Infrared Spectra*, 3rd ed. (Aldrich Chemical Co., Milwaukee, WI, 1981).
[8] H. A. MacKenzie *et al*., Clin. Chem. **45**, 1587 (1999).
[9] G. B. Christison and H. A. McKenzie, Med. Biol. Eng. Comput. **31**, 284 (1993).
[10] W. Martin, S. Mirov, and R. Venugopalan, Appl. Spectrosc. **59**, 881 (2005).
[11] W. Martin, S. Mirov, and R. Venugopalan, J. Biomed. Opt. **7**, 613 (2002).
[12] P. Zheng, C. E. Cramer, C. W. Barnes, J. R. Braig, and B. B. Sterling, Diabetes Technol. Ther. **2**, 17 (2000).
[13] A. Mandelis and X. Guo, US Patent pending No. 12/948,525 (2010).
[14] A. Mandelis, Rev. Sci. Instrum. **65**, 3313 (1994).
[15] Y. Zhang and S. Tadigadapa, in *IEEE Sensors 2005, Proceedings of the Fourth IEEE International Conference on Sensors, Irvine, CA, 2005*, edited by J. Vig, M. Vellekoop, and G. Cauwenberghs (IEEE, Piscataway, NJ, 2005).
[16] *Handbook of Chemistry and Physics*, 70th ed., edited by R. C. Weast and D. R. Lide (CRC Press, Boca Raton, FL, 1989).
[17] R. Darros-Barbosa, M. O. Balaban, and A. A. Teixeira, Int. J. Food Prop. **6**, 239 (2003).
[18] D. M. Wieliczka, S. Weng, and M. R. Querry, Appl. Opt. **28**, 1714 (1989).